Memory cytotoxic SARS-CoV-2 spike protein-specific CD4+ T cells associate with viral control

Tao Dong (tao.dong@imm.ox.ac.uk)
University of Oxford https://orcid.org/0000-0003-3545-3758

Guihai Liu
University of Oxford

Suet Felce
University of Oxford

Xuan Yao
University of Oxford

Zixi Yin
University of Oxford https://orcid.org/0000-0002-2044-5838

Anastasia Fries
University of Oxford https://orcid.org/0000-0003-1609-5991

Alexander Mentzer
University of Oxford https://orcid.org/0000-0002-4502-2209

Danning Dong
University of Oxford

Wenbo Wang
University of Oxford

Wanwisa Dejnirattisai
University of Oxford

Piyada Supasa
University of Oxford

Chang Liu
University of Oxford

Peter Wing
University of Oxford https://orcid.org/0000-0002-2354-3281

Timothy Rostron
University of Oxford

Craig Waugh
University of Oxford

Sally-Ann Clark
University of Oxford https://orcid.org/0000-0003-1720-7975

Kevin Clark

University of Oxford
Paul Sopp
University of Oxford
Philip Hublitz
University of Oxford https://orcid.org/0000-0001-8810-3247
Ryan Beveridge
University of Oxford
Jeremy Fry
ProImmune Limited https://orcid.org/0000-0003-3689-6606
Jane McKeating
University of Oxford
Juthathip Mongkolsapaya
University of Oxford https://orcid.org/0000-0003-3416-9480
Gavin Screaton
University of Oxford https://orcid.org/0000-0002-3549-4309
Graham Ogg
University of Oxford
Julian Knight
University of Oxford
Yanchun Peng
University of Oxford https://orcid.org/0000-0003-2340-0499

Article

Keywords:

Posted Date: February 11th, 2022

DOI: https://doi.org/10.21203/rs.3.rs-1317569/v1

Abstract

Little is known of the role of cytotoxic $CD4^+$ T-cells in the control of viral replication. Here, we investigate $CD4^+$ T-cell responses to three dominant SARS-CoV-2 epitopes and evaluate antiviral activity, including cytotoxicity and antiviral cytokine production. Diverse T cell receptor (TCR) usage including public TCRs were identified; surprisingly, cytotoxic $CD4^+$ T-cells were found to have signalling and cytotoxic pathways distinct from classical $CD8^+$ T-cells, with increased expression of chemokines and tissue homing receptors promoting migration. We show the presence of cytolytic $CD4^+$ T-cells during primary infection associates with COVID-19 disease severity. Robust immune memory 6-9 months post-infection or vaccination provides $CD4^+$ T-cells with potent antiviral activity. Our data support a model where $CD4^+$ killer cells drive immunopathogenesis during primary infection and $CD4^+$ memory responses are protective during secondary infection. Our study highlights the unique features of cytotoxic $CD4^+$ T-cells that use distinct functional pathways, providing preventative and therapeutic opportunities.

Introduction

Understanding the immune phenotype of SARS-CoV-2-specific T cells that are protective or pathogenic is pivotal to define therapeutic and prophylactic strategies to manage the COVID-19 pandemic[1]. Early T cell responses against diverse SARS-CoV-2 proteins associate with clinical protection[2, 3, 4, 5]. In contrast, patients with severe disease have reduced frequencies of circulating T cells and increased activation markers[6, 7, 8, 9, 10, 11, 12]. There is an urgent need to for in-depth functional characterization of virus-specific T cells during natural infection and following vaccination.

In addition to their “helper” role, mainly through interaction with antigen presenting cells and soluble mediators, the direct effector and antiviral function of virus-specific $CD4^+$ T cells have been studied in the setting of several human virus infection settings, such as influenza, cytomegalovirus (CMV) and Epstein-Barr virus (EBV)[13]. $CD4^+$ cytotoxic T cell (CTL) responses were recently recognized to play an important role in the immune response to viral infections. However, most mechanistic studies investigating cytotoxic $CD4^+$ T cells were conducted in murine models; therefore, it is unclear if insights gained from such studies are relevant to human CTL responses[13]. Recent SARS-CoV-2 $CD4^+$ T cell studies have been focused on the regulatory and helper function of these cells, such as T follicular helper cells (Tfh) and their role in assisting antibody production[14, 15]. Very little attention has been paid to the direct effector function and antiviral activity of SARS-CoV-2 specific $CD4^+$ memory T cells, possibly due to the limited experimental tools available.

Current advances in technologies that combine population specific single cell transcriptomic profiling with TCR sequencing analysis and *in vitro* T cell functional assays have enabled us to study the quality of T cell responses and their ability to control virus replication[5]. Multiple immunodominant SARS-CoV-2 spike protein-specific T cell epitopes have been identified and are frequently detected in individuals who have recovered from SARS-CoV-2 infection and following vaccination[16, 17, 18].

In this study we focus on three most dominant $CD4^+$ spike-specific epitopes identified in a cohort of individuals who had recovered from SARS-CoV-2[18]. We explore correlations with the quality of these spike-specific T cell responses and study their TCR repertoires, public TCR usage and their association with antiviral activity. We examine the potential mechanisms of antiviral activity in a specific cytotoxic subset of $CD4^+$ T cells using single cell transcriptome analyses of expanded T cell clones bearing the same TCRs as identified in single cell analysis.

Results

1. Identification of three immunodominant spike-specific $CD4^+$ T cell responses with effector function in individuals recovered from COVID-19

We previously identified three dominant SARS-CoV-2 spike protein (S) $CD4^+$ T cell epitopes: $S_{166-180}$ (CTFEYVSQPFLMDLE), $S_{751-765}$ (NLLLQYGSFCTQLNR) and $S_{866-880}$ (TDEMIAQYTSALLAG)[18]. The HLA-restriction of these epitopes was defined using interferon (IFN)-γ -ELISPOT or peptide-MHC-Class II tetramer staining (Extended Data Fig. 1). $S_{166-180}$-specific T cells are restricted by HLA-DPB1*04:01 and are also detected in vaccinated healthy donors[19]. The remaining two spike epitopes are presented by HLA-DRB1*15:01 as defined by peptide-MHC-Class II tetramer staining. Our cohort includes 45 individuals that had recovered from COVID-19, comprising 26 mild cases and 19 severe cases (including 6 critical cases) based on oxygen requirements during the acute illness (Supplementary Table 1 and Extended Data Fig. 2). Among them, 26 (26/41, 63.41%) were HLA-DPB1*04:01 positive (13 mild and 13 severe cases) and 17 (17/45, 37.78%) carried HLA-DRB1*15:01 (7 mild and 10 severe cases) (Fig. 1a). Our *ex vivo* IFN-γ ELISpot assays with convalescent samples collected 1-3 months post-infection revealed that 68% (17/25) of DPB1*04:01 individuals responded to $S_{166-180}$, while 85.71% (12/14) and 71.43% (10/14) of DRB1*15:01 positive patients showed responses to $S_{751-765}$ and $S_{866-880}$ respectively (Fig. 1b). This further confirmed the immunodominance of these three epitopes. Among $S_{166-180}$ responders, a high proportion of individuals (64.7%, 11/17) had recovered from severe disease (Fig. 1c) and) with significantly stronger responses compared to individuals who had recovered from mild symptoms (P = 0.031; Fig. 1d). Although our data does not provide statistical evidence for an association of $S_{751-765}$- and $S_{866-880}$- specific T cell responses with disease severity, we observed a higher proportion (60%, 6/10) of $S_{866-880}$ responders who had recovered from mild disease (Fig. 1c and d).

To further characterize these three dominant T cell responses, we generated 50 $S_{166-180}$-specific T cell clones, 54 $S_{751-765}$-specific T cell clones and 49 $S_{866-880}$-specific T cell clones from convalescent samples and evaluated their functionality. T cell receptors (TCRs) of each clone were also sequenced (Supplementary Table 2). All clones expressed cytokines including TNF-α, IFN-γ and IL-2 upon antigen activation (Fig. 1e). $S_{866-880}$-specific T cell clones displayed the highest antigen-sensitivity, with the lowest EC_{50} calculated from TNF-α, IFN-γ and IL-2 production. Interestingly, in addition to cytokine expression, we observed a substantial proportion of T cell clones (4 from $S_{166-180}$, 8 from $S_{751-765}$ and

22 from $S_{866-880}$) capable of killing target cells by more than 10%, with the highest level of killing being 60% for $S_{866-880}$ (Fig. 1f). This highlights the existence of SARS-CoV-2-specific $CD4^+$ CTLs following SARS-CoV-2 infection. We defined $CD4^+$ killer cells as clones with a killing capacity of > 10%. Among these spike-specific T cell clones, $S_{866-880}$-specific T cells showed the strongest cytotoxic and killing capacity (Fig. 1f, 61% $P < 0.001$) and proportion of killer cells (Fig. 1g, 60% $P < 0.001$) whereas $S_{166-180}$ T cells showed the least cytotoxic killing potential. The highest effector function and antiviral efficacy was seen for $S_{866-880}$, suggesting significant effector function of cytotoxic $CD4^+$ T cell acting on virus infected cells and controlling virus replication.

2. Spike-specific $CD4^+$ T cell antiviral activity is associated with cytotoxic activity, cytokine production and antigen load

Taking advantage of our *in vitro* SARS-CoV-2 virus infection system[5], we assessed the antiviral activity of these spike-specific $CD4^+$ T cells. In brief, Epstein Barr virus (EBV)-transformed B cell lines (BCLs) ectopically expressing ACE2 were infected with SARS-CoV-2 (Fig. 2a) then cocultured with spike-specific $CD4^+$ T cells. T cell recognition of virus-infected cells was examined by intracellular cytokine staining (ICS), and the suppression of SARS-CoV-2 replication by T cells was assessed by quantifying the number of viral copies in the infected cells after 48hrs of co-culturing. Our data showed that $CD4^+$ T cells targeting these three dominant spike epitopes can recognise virus-infected cells and produce cytokines after activation (Fig. 2b), with $S_{866-880}$-specific-T cells having the highest proportion of TNF-α ($P < 0.001$), IFN-γ ($P < 0.001$) and IL-2 ($P < 0.001$) producing $CD4^+$ T cells after encountering virus-infected BCLs (Fig. 2c). More importantly, $CD4^+$ T cell clones targeting each of the three epitopes exhibited, to varying extents, direct effector function against the virus, capable of suppressing virus replication (Fig. 2d). In particular, T cells targeting $S_{866-880}$ showed significantly better antiviral efficacy compared to T cells targeting epitope $S_{751-765}$ restricted by the same HLA-DRB1*15:01 ($P = 0.002$). We sought to investigate whether this strong antiviral activity was a result of high effector function or exposure to high antigen loads by examining single cell gene expression from tetramer-sorted short term cultured T cell lines. First, we compared single cell gene expression profiles of T cells targeting $S_{751-765}$ ($n = 1629$) and $S_{866-880}$ cells ($n = 2233$) (Fig. 2e). We observed significant upregulation of genes encoding effector molecules, such as cytotoxic molecules *KLRK1* ($P = 1.37 \times 10^{-44}$), *GZMB* ($P = 6.13 \times 10^{-4}$) and *GZMK* ($P = 5.13 \times 10^{-10}$), and cytokines *CCL3* ($P = 2.79 \times 10^{-6}$), *CCL4* ($P = 4.4 \times 10^{-8}$), *TNF* ($P = 9.08 \times 10^{-12}$) in $S_{866-800}$-specific T cells compared to $S_{751-765}$ -specific T cells (Fig. 2f). This further confirms the cytotoxic potential of $S_{866-880}$-specific T cells.

To estimate the antigen load of each epitope on virus-infected cells, we cultured T cells with the same number of target cells either infected with SARS-CoV-2 or loaded with variable amounts of peptide, then assessed T cell responses by ICS (Fig. 2g). The antigen-load in virus-infected cells was equivalent to the peptide concentration that elicited a similar level of response to virus-infected cells. Surprisingly, much lower concentrations (equivalent to 0.06μM) of $S_{866-880}$ peptide were presented on virus-infected cells,

when compared to $S_{166-180}$ (about 0.11μM) and $S_{751-765}$ (equivalent to 2.57μM) (Fig. 2h). Our data suggests that the higher antiviral activity of $S_{866-880}$-specific T-cells is likely to result from cytotoxicity and high antigen sensitivity even when antigen load on the surface of infected cells was relatively low.

Next, we compared the cytotoxic activity of $S_{751-765}$ and $S_{866-880}$ tetramer-sorted short term cultured single cells isolated from those who had recovered from mild or severe acute COVID-19 (n = 2 mild, 2728 cells; n = 2 severe, 1823 cells; Fig. 2i). We observed that T cells isolated from patients who had recovered from severe disease were more activated and expressed higher levels of T cell effector function genes *CD69* ($P = 2.75 \times 10^{-5}$), *CCL5* ($P = 1.61 \times 10^{-22}$), *IL2RG* ($P = 3.27 \times 10^{-35}$), *MX1* ($P = 3.76 \times 10^{-13}$), in particular cytotoxic molecules such as *GZMB* ($P = 6 \times 10^{-17}$) and *GZMM* ($P = 3.87 \times 10^{-3}$), compared to cells from mild cases (Fig. 2j). Collectively, these data suggest that cytotoxic $CD4^+$ T cells may play a role in the immunopathogenesis of the severe disease.

3. Diverse TCR usage and public TCR clonotypes are commonly observed among immunodominant spike T cells

Single cell TCR sequences of *ex vivo* stimulated and cytokine sorted $S_{166-180}$ (n = 152 cells from 5 patients), tetramer-sorted $S_{751-765}$ (n = 77 cells from 4 patients) and tetramer-sorted $S_{866-880}$ (n = 100 cells from 4 patients) -specific T cells from 1-3 months convalescent patients were analysed to assess TCR diversity. Interestingly, each epitope displays a different dominant αV gene usage, with TRAV35, TRAV12-1 and TRAV26-1 being dominant for $S_{166-180}$-, $S_{751-765}$-, and $S_{866-880}$-specific T cells respectively, where each dominant αV gene pairs with multiple different βV genes (Fig. 3a). This highlighted the importance of the α chain in these spike epitope TCRs; hence we decided to focus on the αV chain when investigating TCR clonotypes further. Single cells from epitope specific T cells sampled at different timepoints ($S_{166-180}$ *ex vivo* acute, *ex vivo* 1-3 months, short term culture 9 months convalescence from total 5 patients; $S_{751-765}$ and $S_{866-880}$ *ex vivo* acute, *ex vivo* 1-3 months, short term culture 6 months and 9 months convalescence from total 6 patients) were analysed together to identify public clonotypes (CDR3 amino acid and V gene usage), which are unique clonotypes shared among more than one unrelated patient. We found that public α clonotypes (CDR3α and TRAV) were shared by many patients whereas β clonotypes (CDR3β and TRBV) were shared by a smaller number of patients. For example, the maximum number of patients with one particular α clonotype (CAGTGNNRKLIW, TRAV 25) from $S_{866-880}$-specific T cells could be 6/6 whereas the highest number of patients sharing any β clonotype from the same epitope was 3/6 (Table 1 and Supplementary Table 3). Examination of paired αβ public clonotypes revealed that the β public clonotypes were more diverse than α public clonotypes, with no clear dominant Vβ gene usage for any epitope. By focusing on α clonotypes, we reasoned that we would be better able to study the dominant α V genes for each epitope, which should also capture the diversity of β clonotypes.

Next, we sought to compare the proportion of public and private clonotypes from each epitope. $S_{166-180}$-specific T cells have higher proportions of TCRs matching public clonotypes compared to the other two

epitopes (n = 21 $S_{166-180}$ public α clonotypes, n = 16 $S_{751-765}$ public, n = 19 $S_{866-880}$ public; Fig. 3b). We also investigated if there were any differences between public and private clonotype expansion for each epitope at different timepoints (acute, 1-3 months and 6-9 months convalescence) and found that T cells with public clonotypes were present at higher frequencies compared to cells with private clonotypes, with the exception of $S_{866-880}$ at 6-9 months convalescence (acute: $S_{166-180}$ $P = 1.7 \times 10^{-6}$, $S_{751-765}$ $P = 0.04$, $S_{866-880}$ $P = 0.0098$; 1-3 months: $S_{166-180}$ $P = 1.4 \times 10^{-15}$, $S_{751-765}$ $P = 6.3 \times 10^{-8}$, $S_{866-880}$ $P = 3.8 \times 10^{-6}$; 6-9 months: $S_{166-180}$ $P = 3.1 \times 10^{-9}$, $S_{751-765}$ $P = 0.026$, $S_{866-880}$ $P = 0.15$; Fig. 3c). To further investigate differences between T cells with public and those with private TCRs, we looked at single cell gene expression between these two groups. *Ex vivo* stimulated and cytokine sorted $S_{166-180}$-specific single cells with public TCRs (n =128 cells) had higher expression of activation markers [*IFNG* ($P = 2.92 \times 10^{-5}$), *FASLG* ($P = 9 \times 10^{-8}$), *CD40LG* ($P = 4.86 \times 10^{-16}$), *BTLA* ($P = 1.48 \times 10^{-3}$), *PDCD1* ($P = 1.61 \times 10^{-3}$)], Th1 activators [*ID2* ($P = 1.07 \times 10^{-5}$)] and Th2 suppressors [*NR4A2* ($P = 1.94 \times 10^{-14}$) and *IRF4* ($P = 1.18 \times 10^{-6}$), Fig. 3d] compared with T cells with private TCRs (n = 285 cells). This may indicate that high expansion of T cells with public clonotypes might drive a Th1 response in convalescent COVID-19 patients. Conversely, tetramer-sorted $S_{866-880}$-specific T cells from short term culture with private TCRs (n = 1325 cells) display higher expression of cytotoxic genes [*KLRK1* ($P = 5.65 \times 10^{-8}$), *GZMA* ($P = 1.22 \times 10^{-3}$), *GZMK* ($P = 2.95 \times 10^{-5}$), *NKG7* ($P = 3.92 \times 10^{-4}$), *CCL5* ($P = 1.19 \times 10^{-8}$), Fig. 3e] compared with T cells with public TCRs (n = 194 cells). Similar results were observed with $S_{751-765}$-specific T cells (Extended Data Fig. 3). In summary, these results highlight the potential different functional activities between epitope-specific T cells.

4. Cytotoxicity and function of spike-specific CD4 $^{+}$ T cells are regulated by more than TCR usage alone.

We next investigated whether the effector function of spike-specific $CD4^+$ T cells was due to their broad TCR usage by comparing antigen sensitivity and killing capacity of T cell clones bearing the same TCR. We found that T cells with the same TCRs had very different antigen sensitivities, reflected in a wide range of EC_{50} values for IFN-γ, TNF-α and IL-2 production (Fig. 4a). These T cell clones also produced different cytokine profiles upon antigen stimulation (Extended Data Fig. 4). Moreover, $S_{866-880}$-specific T cell clones with shared TCRs had distinct killing capacities (Fig. 4b), for example, clone 2 had 40% killing capacity while clone 3 showed minimal killing despite sharing the same TCR (TRAV12-1/TRBV5-1). This suggested that the cytolytic activity of these spike-specific $CD4^+$ T cells was due to factors beyond TCR usage. This observation was further confirmed by variable expression levels of cytotoxic molecule genes, such as *PRF1*, *GZMA* and *GZMB*, in tetramer-sorted $S_{866-880}$ single cells (n = 399 cells) with the same TCR usage (Fig. 4c). Indeed, we noted a positive association between killing ability with degranulation activity, as measured by CD107a expression, upon antigen stimulation (R = 0.413, P = 0.001, Fig. 4d). This suggests that high expression of CD107a can act as a potential marker for $CD4^+$ CTLs.

5. Antiviral activity of spike-specific CD4 $^{+}$ T cells strongly correlates with their killing capacity and IL-2 production

As previously highlighted, a number of spike-specific $CD4^+$ T cell clones were capable of suppressing virus replication (Fig. 2d). We further examined whether this antiviral effector function was mediated via direct killing of virus-infected cells or by the expression of soluble inhibitory factors. Firstly, our data demonstrated that the antiviral activity of the $CD4^+$ T cell clones strongly correlated to the proportion of cells producing IL-2 upon stimulation with virus-infected cells (R = 0.226, P = 0.030, Fig. 5a), but did not correlate with the proportion of cells producing IFN-γ or TNF-α (Extended Data Fig. 5). Secondly, we found a significant association between the killing capacity of T cells and their potential to control virus replication. Indeed, we observed that killer cells (more than 10% killing capacity) could suppress virus replication more efficiently than non-killers (less than 10% of killing) (Fig. 5b R = 0.390, P < 0.001), suggesting the importance of direct killing of virus-infected cells in viral control by $CD4^+$ CTLs. Strikingly, some non-killer cells were capable of inhibiting viral replication as efficiently as killer cells, indicating the potential contribution of soluble factors to viral control (Fig. 5c). Subsequently we compared cytokine and chemokine production of these viral suppressing non-killer $CD4^+$ T cells with other non-killer cells (Fig. 5d). We noticed that non-killer $CD4^+$ T cells capable of suppressing virus replication (suppressor clone) produced significantly higher concentrations of IL-2 (P = 0.040) and IFN-γ (P = 0.040) than non-killer $CD4^+$ T cells incapable of viral suppression (non-suppressor clone), highlighting a role for IL-2 and possibly IFN-γ in $CD4^+$ T cell control of SARS-CoV-2 infection.

6. Cytotoxic spike-specific $CD4^+$ CTLs utilise distinct cytolytic pathways with increased migration potential

Activated $CD8^+$ CTLs carry out their killing function primarily by releasing cytotoxic granules such as perforin and granzymes, which subsequently induce apoptosis of target cells. To determine whether the killing of target cells by spike-specific $CD4^+$ CTLs was also mediated through the perforin-dependent pathway, $S_{866-880}$-specific $CD4^+$ T cell clones were treated with concanamycin A (CMA), an inhibitor of perforin, prior to adding to target cells loaded with peptide. The cytolytic activity mediated by $CD4^+$ T cell clones was completely blocked by CMA, resulting in decreased or ablated killing capacity (Fig. 6a), and reduced or no viral suppression (Fig. 6b). To identify other factors involved with this perforin-mediated effective viral control, we grouped tetramer-sorted $S_{866-880}$-specific single cells from short term cultured lines into perforin-high (n = 693 cells) and perforin-low (n = 724 cells) subsets according to their perforin module scores (Supplementary Table 4) and compared their gene expression profiles (Fig. 6c). Perforin-high T cells not only upregulate cytotoxic associated genes such as *GZMA* (P = 4.43 x 10^{-144}), *NKG7* (P = 1.03 x 10^{-139}), *GZMK* (P = 4.34 x 10^{-39}), *KLRD1* (P = 2.01 x 10^{-2}) and *CTSW* (P = 6.54 x 10^{-35}) but also genes associated with migration for example: chemokines such as *CCL3* (P = 8.48 x 10^{-16}), *CCL4* (P = 2.26 x 10^{-59}), *CCL5* (P = 9.29 x 10^{-82}), chemokine receptors *CCR3* (P = 4.6 x 10^{-3}) and *IL2RG* (P = 3.17 x 10^{-24}), tissue homing receptors *ITGB1* (P = 1.19 x 10^{-8}), *ITGA4* (P = 1.26 x 10^{-3}), *ITGAL* (P = 3.78 x 10^{-4}) and inhibitory receptors such as *TIGIT* (P = 2.82 x 10^{-4}) and *KLRG1* (P = 1.94 x 10^{-2}) (Fig. 6d). This suggests there is increased migration potential of activated cytotoxic $CD4^+$ T cells to infected tissue.

To understand whether these spike-specific $CD4^+$ CTLs utilise similar cytolytic pathways as $CD8^+$ CTLs, we compared single cell gene expression, in particular the expression of effector molecules, between perforin-high $CD4^+$ cytotoxic T cells (tetramer-sorted $S_{866-880}$ specific, *n* = 693) and $CD8^+$ cytotoxic T cells (Pentamer-sorted HLA-B*0702/$NP_{105-113}$-specific, *n* = 1041) from short term cultured lines[5] (Fig. 6e). We found that $CD8^+$ CTLs expressed significantly higher levels of granzyme B and H (*GZMB*, average $\log_2$ fold change = -2.68, $P = 2.24 \times 10^{-25}$; *GZMH*, average $\log_2$ fold change = -0.57, $P = 2.09 \times 10^{-5}$), classic cytolytic molecules secreted by $CD8^+$ T cells and induce apoptosis in target cells (Fig. 6f). Compared to $CD8^+$ CTLs, $CD4^+$ CTLs displayed upregulated expression of other cytolytic molecules such as *GZMM* ($P = 1.91 \times 10^{-10}$), *GZMK* ($P = 1.78 \times 10^{-10}$), *NKG7* ($P = 9.51 \times 10^{-12}$), *KLRK1* ($P = 8.3 \times 10^{-6}$) and *CTSW* ($P = 2.86 \times 10^{-11}$), suggesting the involvement of different cytolytic machineries in $CD4^+$ CTL killing.

7. Dominant spike-specific $CD4^+$ T cells are maintained nine months after infection with diverse TCR repertoire and preserved antiviral activity.

To examine whether memory T cells established following natural infection could provide sufficient protection against secondary viral infection, we collected peripheral blood mononuclear cells (PBMCs) from the same patients 6-9 months after infection. Although T cell responses to these three spike epitopes ($S_{166-180}$, $S_{751-765}$ and $S_{866-880}$) significantly declined six months after infection (Fig. 7a), we were able to sort, sequence, and expand these spike-specific $CD4^+$ T cells after *in vitro* antigen stimulation. We discovered that the diversity of the TCR repertoire of these $CD4^+$ T cells were maintained 6-9 months after infection (Fig. 7b). We then assessed the antiviral efficacy of these bulk spike-specific T cell lines using our *in vitro* SARS-CoV-2 infection assays. The bulk lines targeting all three epitopes elicited strong responses against BCLs infected with SARS-CoV-2 (Victoria strain) and variants of concerns (VOCs; Delta and Omicron). The $CD4^+$ T cell lines produced profoundly elevated level of IFN-γ, TNF-α and IL-2 (Fig. 7c and Extended Fig. 6) and showed significant cytotoxic potential with upregulated CD107a expression (Fig. 7d). In addition, we found that these antigen-specific $CD4^+$ bulk cell lines are capable of suppressing SARS-CoV-2 replication and showed strong inhibition against VOCs (Fig. 7e). Our data highlight the protective role of these dominant spike-specific $CD4^+$ T cells in secondary infection against different SARS-CoV-2 variants.

Discussion

In this study, we focus on the three most dominant spike-specific $CD4^+$ T cell responses identified in our cohort restricted by common HLA Class II alleles ($S_{166-180}$-DPB1*04:01, $S_{751-765}$-DRB1*15:01 and $S_{866-880}$-DRB1*15:01). Significant differences are observed between these responses in functional avidity/antigen sensitivity, cytotoxic capacity, cytokine profile and their effector function in response to virus infected cells and suppression of virus replication. $S_{866-880}$ specific T cells show the strongest responses to virus infected cells and direct control of virus replication, which was associated with potent cytotoxic capacity and high antigen sensitivity to cytokine production, such as IL-2. $S_{166-180}$ responses

feature dominant public TCR usage, in particular TRAV35, that is biased to TH1 cell subset[20] (i.e. high *ID2* expression) and suppressed TH2 transcriptomic profiles[21] (i.e. high TH2 suppressor *IRF4* and *NR4A2* expression). TCR repertoire analysis surprisingly reveals that over 30% of TCRs are public in all three epitope specific responses at all time points studied, including public clonotypes with shared αV and βV sequences. There are also different dominant TRAV usages across these three epitope specific T cells, with $S_{166-180}$ dominated by TRAV35, $S_{751-765}$ by TRAV12-1 and $S_{866-880}$ by TRAV25, TRAV26-1 and TRAV12-1 clonotypes.

Interestingly, the estimated antigen load from antigen sensitivity assays and virus suppression assays reveals significant differences among these three epitopes. Despite over 10 times less estimated $S_{166-180}$ epitope peptide loaded on the MHCII of infected cells than $S_{751-765}$, $S_{166-180}$ and $S_{751-765}$ have similar antiviral activity for both cytokine production and direct viral control. The fact that $S_{166-180}$ responses display much higher overall antigen sensitivity than $S_{751-765}$ may compensate the lower antigen load on the cell surface. $S_{866-880}$ displays the strongest antiviral responses and antigen sensitivity among all three epitope responses, despite having the lowest antigen load. These results suggest that both antigen sensitivity and viral load on infected cells or antigen presenting cells are likely to play critical roles in viral control by these spike-specific $CD4^+$ T cells, and need to be considered carefully when peptide-based approaches are only used to measure T cell responses.

$CD4^+$ cytotoxic T cell responses observed in virus infection and cancer may contributed to disease pathogenesis[22, 23] or protection[24, 25, 26]. We observe potent cytotoxic capacity and antiviral efficacy of $S_{866-880}$ CD4+ T cells. Looking further into this response, we first find that cytotoxicity is likely primarily mediated by perforin, which is in agreement with previous reports[27, 28, 29]. When we compare cells at a single cell level, we find a significant association of $CD4^+$ cytotoxic T cells in individuals recovered from severe in comparison with mild disease; however, the number of patients studied are small, therefore further large-scale studies are needed. Using single cells with high and low perforin scores as a marker for $CD4^+$ cytotoxic T cells, we find that perforin-high cells have the potential to migrate to affected tissue efficiently by expressing high levels of chemokines (*CCL3*, *CCL4* and *CCL5*) and tissue homing receptors (*ITGB1*, *ITGA4* and *ITGAL*), in line with the observation that $CD4^+$ CTLs are expanded in the lung of patients with severe COVID-19[30]. Our data highlights the potential pathogenic role of these potent cytotoxic T cells during primary virus infection. These cells may accumulate in the infected organ/tissue, causing excessive inflammation and bystander killing of cells with elevated MHC Class II expression, including professional antigen presenting cells. This hypothesis merits further investigation.

We also find that cytotoxic $CD4^+$ T cells may use different signalling and cytotoxic molecules compared to classical $CD8^+$ T cells; $CD4^+$ CTLs express *GZMK* and *GZMM* significantly higher whereas $CD8^+$ CTLs express much higher *GZMB* and *GZMH*. In addition, NK activation receptor NKG2D (*KLRK1*) and NKG7, known to be important for cytotoxic degranulation[31], are highly expressed on $CD4^+$ CTLs but not classical $CD8^+$ CTLs.. Importantly, it is known that NKG2D ligands are expressed in the lung affected by COVID-19,

therefore the high NKG2D expression on cytotoxic $CD4^+$ T cells could potentially contribute to potent cytotoxicity in infected lungs and provide additional protection in mild COVID-19 cases or excessive inflammation in severe cases.

Surprisingly, we find that the functionality of these $CD4^+$ T cells, in particular cytotoxicity, appears to involve mechanisms beyond TCR usage alone. $S_{866-880}$ –specific T cell clones sharing the same TCR exhibit a broad range of killing capacity, which correlate with their ability to control virus replication in infected cells. However, T cells with no killing activity can still suppress virus replication and express high levels of IL-2 and IFN-γ. In addition, we observe an overall significant association between IL-2 and IFN-γ and the antiviral efficacy of all three epitope responses, suggesting direct antiviral effector function of $CD4^+$ spike-specific T cells independent of cytotoxicity.

Finally, the immune memory responses from 6 - 9 months post-infection demonstrate potent antiviral efficacy to the original SARS-CoV-2, Delta and Omicron Variants, suggesting memory responses to spike protein, induced by vaccine or natural infection, may contribute to protection against secondary infections to all VOCs, including Omicron, by direct killing of virus infected cells and/or antiviral cytokine and chemokine production.

In summary, our study provides evidence of cytotoxic $CD4^+$ T cells in SARS-CoV-2 virus infection and new insights on the potential mechanisms related to this important group of $CD4^+$ cells at a single cell level. Induction of potent $CD4^+$ killer cells by vaccination could be an attractive approach for novel vaccine designs to support early viral control.

Declarations

Acknowledgments:

We are grateful to all the participants for donating their samples and data for these analyses, and the research teams involved in the consenting, recruitment, and sampling of these participants. The manuscript was edited at Life Science Editors.

This work is supported by Chinese Academy of Medical Sciences (CAMS) Innovation Fund for Medical Sciences (CIFMS), China (grant number: 2018-I2M-2-002) (T.D, Y.P, S.L.F, X.Y, G.L, D.D, J.C.K, G.O, G.R.S); UK Medical Research Council (T.D, G.O, Y.P); National Institutes of Health, National Key R&D Program of China (2020YFE0202400) (T.D); China Scholarship Council (Z.Y, G.L, C.L). The study is also funded by the NIHR Oxford Biomedical Research Centre (G.O, J.C.K), Wellcome Trust Investigator Award (204969/Z/16/Z) (J.C.K), Wellcome Trust Grants (090532/Z/09/Z and 203141/Z/16/Z) to core facilities Wellcome Centre for Human Genetics, Senior Investigator Award (G.O) and Clinical Research Network (G.O); Schmidt Futures (G.R.S), The McKeating laboratory is funded by a Wellcome Investigator Award (IA) 200838/Z/16/Z, UK Medical Research Council (MRC) project grant MR/R022011/1.

This work uses data provided by patients and collected by the NHS as part of their care and support #DataSavesLives.

Author contributions:

T.D conceptualized the project; T.D and Y.P designed and supervised T cell experiments; J.C.K supervised bioinformatic analysis, G.L,Y.P, X.Y, Z.Y, D.D and W.W performed all T cell experiments and data analysis; S.L.F performed single cell data analysis; P.A.C.W and J.A.M assisted with virus infection; T.R performed HLA typing and next generation sequencing; P.H and R.B made the ACE2 constructs and lentivirus; J.W.F provided MHC Class II Tetramers; J.C.K, A.J.M, A.F established clinical cohorts and collected clinical samples and data; C.W, S-A.C, K.C, P.S, W.D, P.S, C.L, J.M, G.R.S provided technical assistance and critical reagents; T.D, J.C.K and Y.P supervised data analysis, T.D , Y.P, G.L, S.L.F, wrote the original draft. J.C.K, G.O and S.L.F reviewed and edited the manuscript and figures.

Competing interests: The authors declare no competing interests.

Data and materials availability: All data are available in the main text or the supplementary materials.

Methods

Study participants and clinical definitions. Patients were recruited from the John Radcliffe Hospital in Oxford, UK, between March 2020 and September 2021 by identification of patients hospitalized during the SARS-CoV-2 pandemic and recruited into the Sepsis Immunomics study. Patients were sampled at least 28 days after symptom onset. Written informed consent was obtained from all patients. Ethical approval was given by the South Central-Oxford C Research Ethics Committee in England (ref. 19/SC/0296). Clinical definitions were defined as previously described[1].

Generation of ACE2-transduced EBV-transformed BCLs. EBV-transformed BCLs[32] and ACE2-transduced BCLs[5] were established as described previously. In brief, the cDNA for the human *ACE2* gene (ENSG00000130234) was cloned into a lentiviral vector backbone (Addgene plasmid ID 17488), then co-transfected with packaging plasmids pMD2.G and psPAX2 into HEK293-TLA using PEIpro (Polyplus) to produce lentivirus. EBV-transformed BCLs were infected with ACE2-coding lentivirus followed by cell sorting via flow cytometry to enrich ACE2-expressing B cells. B cells with stable expression of ACE2 were maintained with 0.5 μg ml^{-1} of puromycin (Thermo Fisher Scientific). *Mycoplasma* testing was carried out every 4 weeks with all cell lines using MycoAlert detection kit (Lonza).

Generation of T cell lines and clones. Short-term SARS-CoV-2-specific T cell lines were generated as described previously[33]. Briefly, 2 x 10^6 PBMCs were pulsed with 10 μM peptides at 37°C for 1hr and cultured in R10 (RPMI 1640 medium with 10% human serum, 2 mM glutamine and 100 mg ml^{-1} of penicillin–streptomycin) at 2 x 10^6 cells per well in a 24-well plate (Costar). IL-2 was added to a final concentration of 100 IU ml^{-1} on day3. $S_{751\text{-}765}$- and $S_{866\text{-}880}$-specific T cell clones were established by

sorting tetramer$^+$ CD4$^+$ T cells from thawed PBMCs or short-term T cell lines on day 10-14. $S_{166-180}$-specific T cell clones were generated by cell sorting with TNF-α, IFN-γ, and IL-2 secretion assay (Miltenyi). T cell clones were then expanded with irradiated allogeneic PBMCs every 2-3 weeks as described previously[34].

IFNγ ELISpot assay. *Ex vivo* assays were carried out using either freshly isolated or cryopreserved PBMCs as described previously[18]. Peptides were added to 2 x 10^5 PBMCs at a final concentration of 2 μM for 16-18hrs. For *in vitro* ELISpot assays, autologous and allogeneic EBV-transformed BCLs were loaded with peptides, and subsequently cocultured with T cell clones or bulks at an effector:target (E:T) ratio of 1:50 for at least 6hrs. To quantify antigen-specific responses, mean spots of the control wells were subtracted from the sample wells, and the results expressed as spot forming units (SFU) per 10^6 PBMCs. Responses were considered positive if results were at least 3x the mean of the quadruplicate negative control wells and >25 SFU/10^6 PBMCs. If negative control wells had >30 SFU/10^6 PBMCs or positive control wells (PHA stimulation) were negative, the results were excluded from further analysis.

Cell sorting for single cell RNA sequencing (scRNA-seq). $S_{166-180}$-specific CD4$^+$ T cells were sorted using cytokine secretion assay following the manufacturer's instructions (Miltenyi Biotec). Briefly, 1-3 x 10^6 cells were stimulated with $S_{166-180}$ peptide at a final concentration of 10 μM for 5hrs. Subsequently, cells were washed and incubated with TNF-α, IFN-γ, and IL-2 catching antibody for 45 mins, followed by staining with CD3-BV785 (BioLegend), CD4-APC, CD14-PE-CF594, CD19-PE-CF594 and CD16-PE-CF594 (BD Biosciences). Before sorting, cells were stained with Propidium Iodide (PI) (eBioscience) to exclude nonviable cells. $S_{751-765}$- and $S_{866-880}$- specific CD4$^+$ T cells were sorted with peptide-Class II tetramers. In brief, 1-3 x 10^6 cells were stained with APC-conjugated HLA-DRB1*15:01 $S_{751-765}$ and $S_{866-880}$ tetramers (ProImmune) respectively. Live/dead fixable Aqua dye (Invitrogen) was used to exclude nonviable cells from the analysis. Cells were washed and stained with the following surface antibodies: CD4-PE (BD Biosciences), CD3-BV785, CD14-BV510, CD19-BV510 and CD16-BV510 (BioLegend). After exclusion of nonviable/CD14$^+$/CD19$^+$/CD16$^+$cells, CD3$^+$CD4$^+$TNF-α$^+$/IFN-γ$^+$/IL-2$^+$ cells or CD3$^+$CD4$^+$Tetramer$^+$ were sorted for scRNA-seq using a BD FACSAria Fusion sorter or BD FACS Aria III (BD Biosciences). Single cells were directly sorted into 96-well PCR plates (Thermo Fisher Scientific) and stored at −80°C for further SmartSeq2 analysis as described previously[5]; bulk cells were sorted into 1.5ml Eppendorf tubes (Eppendorf) for subsequent Chromium Single Cell Immune Profiling analysis following manufacturer's instruction (10x Genomics).

SmartSeq2 scRNA-seq data processing. BCL files were converted to FASTQ format using bcl2fastq v2.20.0.422 (Illumina). FASTQ files were aligned to human genome hg19 using STAR v2.6.1d. Reads were counted using featureCounts (subread v2.0.0). The resulting counts matrix was analyzed in R v4.0.1 using Seurat v4.0.1.

10x scRNA-seq data processing. BCL files were converted to FASTQ files using cellranger mkfastq (Cellranger v.5.0.0). Counts matrices and sample demultiplexing was carried out using cellranger count

(CellRanger) using with Feature Barcode options. For additional donor deconvolution, cellSNP v.0.3.2 was used to generate a list of SNPs from Cellranger output (BAM files), followed by Vireo v.0.5.6 to demultiplex sequencing data into individual patients from pooled sequenced libraries. The resulting counts matrix was analyzed in R using Seurat.

Single cell RNA sequencing analysis. Cells were filtered using the following criteria: minimum number of cells expressing specific gene = 3, minimum number of genes expressed by cell = 200 and maximum number of genes expressed by cell = 4000. Cells were excluded if they expressed more than 5 – 10% mitochondrial genes. Patient-specific cells were integrated using Harmony v.1.0 to remove batch effects. The AddModuleScore function (Seurat) was used to look at the expression of specific gene sets (Supplementary Table 4). The average expression of a gene set was calculated, and the average expression levels of control gene sets were subtracted to generate a score for each cell relating to that particular gene set. Higher scores indicate that that specific signature is more highly expressed in a particular cell compared with the rest of the population. Cells with a module score ≥ 1 were defined as perforin-high; cells with a score ≤ 0.25 were defined as perforin-low. The FindMarkers function (Seurat) was used to evaluate differentially expressed genes (DEGs) between two conditions using MAST (Model-based Analysis of Single Cell Transcriptomics) statistical test, with different sequencing batches as latent variables. DEGs were visualized on volcano plots using EnhancedVolcano v1.6.0 and VlnPlot (Seurat).

SmartSeq2 and 10x TCR processing. TCR sequences were reconstructed from SmartSeq2 scRNA-seq FASTQ files using MiXCR v.3.0.13 to produce separate TRA and TRB output files for analysis. The output files were parsed into R using tcR v.2.3.2. TCR sequences were extracted from 10x VDJ sequencing using cellranger vdj (Cellranger). The resulting filtered_contig_annotations.csv file was analysed in R.

Single cell TCR repertoire analysis. TCRs were filtered to retain 1/2α or 1β; paired αβ cells consist of 1α1β or 2α1β. Clonotypes were defined as α (CDR3α amino acid + TRAV), β (CDRβ amino acid +TRBV) or paired αβ (CDR3α amino acid + TRAV + CDRβ amino acid +TRBV). Public clonotypes were defined as shared clonotypes between 2 or more patients. Circo plots were plotted using circlize v.0.4.12 showing paired TRAV-TRBV. Pie charts showing α clonotypes were plotted using ggplot2 v.3.3.2. Box plots comparing public/private clonotypes were plotted using ggplot2 and ggpubr v.0.4.0. Longitudinal TCRs were represented graphically using ggalluvial v.0.12.2.

Deep sequencing of TCR repertoire of T cell clones. TCR usage of T cell clones was sequenced as described[5]. Total RNA was extracted from 5×10^5 cells of each clone using RNeasy Micro Kit (QIAGEN), and 100-300ng of the RNA from each clone was used for the generation of full-length TCR repertoire libraries using SMARTer Human TCR a/b Profiling Kit/v2 (TAKARA) following the supplier's instruction. After purification, libraries of all clones were pooled and sequenced using MiSeq reagent Kit v.3 (600 cycles) on MiSeq (Illumina) with MiSeq Control Software v.2.6.2.1. Sequencing BCL files were converted to FASTQ files using bcl2fastq. TCRs were extracted using MiXCR and parsed into R as described earlier. TCRs were filtered to retain 1α1β or 2α1β for each clone.

Intracellular cytokine staining. Intracellular cytokine staining (ICS) was performed as described previously[18]. T cells were cocultured with peptide-pulsed or virus-infected BCLs at 37°C for 6hrs with GolgiPlug and GolgiStop then stained with CD107a-PE (BD Bioscience). Cells were stained with Live/Dead Fixable Aqua dye (Invitrogen) followed by surface staining with CD4-PE-Cy7 (BD, Biosciences). After subsequent permeabilisation with Fixation/Permeabilisation solution (BD, Biosciences), cells were stained with IFN-γ-AF488 (BD Biosciences), TNF-α-APC (eBioscence) and IL-2-BV421 (BioLegend). Negative controls without peptide or without virus infection were set up for each sample. Samples were run on Attune NxT Flow Cytometer (software v.3.2.1) and analysed using FlowJo v.10 software (FlowJo LLC).

CFSE-based cytotoxic T lymphocyte killing assay. EBV-transformed BCLs were labelled with 0.5 μM carboxyfluoroscein succinimidyl ester (CFSE, ThermoFisher) then pulsed with 10 μM of peptide at 37°C for 1hr. Subsequently, cells were washed, counted and cocultured with T cells at an E:T ratio of 4:1 at 37°C for 6hrs. Samples were then stained with 7-AAD (eBioscience) and CD19-BV421 (BioLegend). Cell death was assessed based on the presence of $CFSE^{+}CD19^{+}$7-AAD- (live) cells. Negative controls containing BCLs without peptide pulse and T cells were included for each sample. Samples were run on Attune NxT Flow Cytometer (software v.3.2.1) and analysed using FlowJo v.10 software (FlowJo LLC).

T cell responses to live SARS-CoV-2 infection. SARS-CoV-2 was propagated and titrated as previously described[5]. The Omicron variant was provided by G. Screaton[35]. AEC2-transduced BCLs were infected with SARS-CoV-2 viruses at MOI 0.1 for 2hrs at 37°C, after which cells were washed and incubated at 37°C for 24hrs. Subsequently, cells were washed and cocultured with T cells at an E:T ratio of 1:1. CD107a expression and cytokine production of T cells were evaluated by ICS as described above.

Live virus suppression assay. As described previously[5], BCLs expressing ACE2 were infected with SARS-CoV-2 viruses at MOI 0.1 for 2hrs at 37°C. Cells were then washed and cocultured with T cells at an E:T ratio of 4:1 at 37°C. Control wells containing only virus-infected targets were included. After 48hrs incubation, cells were washed with PBS and lysed with RLT buffer (QIAGEN), followed by RNA extraction using RNeasy 96 Kit (QIAGEN). Virus copies were quantified using real-time qPCR, and the virus suppression rate was calculated by the reduction of viral copies when antigen-specific T cells present.

Statistical analysis. EC_{50} calculations were performed with GraphPad Prism 9, all other statistics were analyzed with IBM SPSS Statistics 27. Figures were made with GraphPad Prism 9. Chi-square was used to compare ratio difference between two groups. Data distribution normality was examined with Kolmogorov-Smirnov test. Mann-Whitney U test was employed to compare two groups, and Kruskal-Wallis one-way ANOVA was used to compare three groups. Correlation analysis was performed using Spearman's rank correlation coefficient. EC_{50} of T cell clones was calculated by using nonlinear regression with variable slope (four parameters) in a dose–response–stimulation model with GraphPad Prism. Statistical significance was set at $P<0.05$ and all tests were 2-tailed. For statistical analyses conducted using R, MAST test was used to find DEGs between two conditions, taking into account variation in batches and represented by volcano plots and violin plots (adjusted *P* value shown). A Mann-

Whitney nonparametric U-test was used for comparison between groups of public/private clonotypes (boxplots), the adjusted *P* value is shown (Benjamini-Hochberg). ns, not significant; * $P < 0.05$, ** $P < 0.01$, *** $P < 0.001$, **** $P < 0.0001$.

References

1. Bertoletti, A., Le Bert, N., Qui, M. & Tan, A.T. SARS-CoV-2-specific T cells in infection and vaccination. Cell Mol Immunol **18**, 2307–2312 (2021).
2. Bergamaschi, L. *et al.* Longitudinal analysis reveals that delayed bystander CD8+ T cell activation and early immune pathology distinguish severe COVID-19 from mild disease. Immunity **54**, 1257-1275 e1258 (2021).
3. Tan, A.T. *et al.* Early induction of functional SARS-CoV-2-specific T cells associates with rapid viral clearance and mild disease in COVID-19 patients. Cell Rep **34**, 108728 (2021).
4. Notarbartolo, S. *et al.* Integrated longitudinal immunophenotypic, transcriptional and repertoire analyses delineate immune responses in COVID-19 patients. Science immunology **6** (2021).
5. Peng, Y. *et al.* An immunodominant NP105-113-B*07:02 cytotoxic T cell response controls viral replication and is associated with less severe COVID-19 disease. Nat Immunol **23**, 50–61 (2022).
6. Arunachalam, P.S. *et al.* Systems biological assessment of immunity to mild versus severe COVID-19 infection in humans. Science (New York, N.Y.) **369**, 1210–1220 (2020).
7. Hadjadj, J. *et al.* Impaired type I interferon activity and inflammatory responses in severe COVID-19 patients. Science (New York, N.Y.) **369**, 718–724 (2020).
8. Kuri-Cervantes, L. *et al.* Comprehensive mapping of immune perturbations associated with severe COVID-19. Science immunology **5**, eabd7114 (2020).
9. Laing, A.G. *et al.* A dynamic COVID-19 immune signature includes associations with poor prognosis. Nat Med **26**, 1623–1635 (2020).
10. Mann, E.R. *et al.* Longitudinal immune profiling reveals key myeloid signatures associated with COVID-19. Science immunology **5** (2020).
11. Mathew, D. *et al.* Deep immune profiling of COVID-19 patients reveals distinct immunotypes with therapeutic implications. Science (New York, N.Y.) **369** (2020).
12. Su, Y. *et al.* Multi-Omics Resolves a Sharp Disease-State Shift between Mild and Moderate COVID-19. Cell **183**, 1479-1495 e1420 (2020).
13. Juno, J.A. *et al.* Cytotoxic CD4 T Cells-Friend or Foe during Viral Infection? Front Immunol **8**, 19 (2017).
14. Shaan Lakshmanappa, Y. *et al.* SARS-CoV-2 induces robust germinal center CD4 T follicular helper cell responses in rhesus macaques. Nat Commun **12**, 541 (2021).
15. Boppana, S. *et al.* SARS-CoV-2-specific circulating T follicular helper cells correlate with neutralizing antibodies and increase during early convalescence. PLoS Pathog **17**, e1009761 (2021).

16. Low, J.S. *et al.* Clonal analysis of immunodominance and cross-reactivity of the CD4 T cell response to SARS-CoV-2. Science (New York, N.Y.) **372**, 1336–1341 (2021).
17. Painter, M.M. *et al.* Rapid induction of antigen-specific CD4(+) T cells is associated with coordinated humoral and cellular immunity to SARS-CoV-2 mRNA vaccination. Immunity **54**, 2133-2142 e2133 (2021).
18. Peng, Y. *et al.* Broad and strong memory CD4(+) and CD8(+) T cells induced by SARS-CoV-2 in UK convalescent individuals following COVID-19. Nat Immunol **21**, 1336–1345 (2020).
19. Mudd, P.A. *et al.* SARS-CoV-2 mRNA vaccination elicits a robust and persistent T follicular helper cell response in humans. Cell (2021).
20. Han, X. *et al.* ID2 and ID3 are indispensable for Th1 cell differentiation during influenza virus infection in mice. Eur J Immunol **49**, 476–489 (2019).
21. Zheng, Y. *et al.* Regulatory T-cell suppressor program co-opts transcription factor IRF4 to control T(H)2 responses. Nature **458**, 351–356 (2009).
22. Hashimoto, K. *et al.* Single-cell transcriptomics reveals expansion of cytotoxic CD4 T cells in supercentenarians. Proc Natl Acad Sci U S A **116**, 24242–24251 (2019).
23. Crompton, L., Khan, N., Khanna, R., Nayak, L. & Moss, P.A. CD4+ T cells specific for glycoprotein B from cytomegalovirus exhibit extreme conservation of T-cell receptor usage between different individuals. Blood **111**, 2053–2061 (2008).
24. Soghoian, D.Z. *et al.* HIV-specific cytolytic CD4 T cell responses during acute HIV infection predict disease outcome. Science translational medicine **4**, 123ra125 (2012).
25. Johnson, S. *et al.* Cooperativity of HIV-Specific Cytolytic CD4 T Cells and CD8 T Cells in Control of HIV Viremia. J Virol **89**, 7494–7505 (2015).
26. Wilkinson, T.M. *et al.* Preexisting influenza-specific CD4+ T cells correlate with disease protection against influenza challenge in humans. Nat Med **18**, 274–280 (2012).
27. Appay, V. *et al.* Characterization of CD4(+) CTLs ex vivo. J Immunol **168**, 5954–5958 (2002).
28. Brown, D.M., Lee, S., Garcia-Hernandez Mde, L. & Swain, S.L. Multifunctional CD4 cells expressing gamma interferon and perforin mediate protection against lethal influenza virus infection. J Virol **86**, 6792–6803 (2012).
29. McKinstry, K.K. *et al.* Memory CD4+ T cells protect against influenza through multiple synergizing mechanisms. J Clin Invest **122**, 2847–2856 (2012).
30. Kaneko, N. *et al.* Expansion of Cytotoxic CD4+ T cells in the lungs in severe COVID-19. *medRxiv* (2021).
31. Malarkannan, S. NKG7 makes a better killer. Nature Immunology **21**, 1139–1140 (2020).
32. Dong, T. *et al.* HIV-specific cytotoxic T cells from long-term survivors select a unique T cell receptor. J Exp Med **200**, 1547–1557 (2004).
33. de Silva, T.I. *et al.* The impact of viral mutations on recognition by SARS-CoV-2 specific T cells. iScience **24**, 103353 (2021).

34. Abd Hamid, M. *et al.* Self-Maintaining CD103(+) Cancer-Specific T Cells Are Highly Energetic with Rapid Cytotoxic and Effector Responses. Cancer Immunol Res **8**, 203–216 (2020).

35. Dejnirattisai, W. *et al.* SARS-CoV-2 Omicron-B.1.1.529 leads to widespread escape from neutralizing antibody responses. Cell (2022).

Tables

Table 1 | Public TCR clonotypes for each spike epitope.

Epitope	CDR3α	TRAV	No. of patients
$S_{166-180}$	CAALNYGGSQGNLIF	TRAV35	5/5
	CAGLLFKAAGNKLTF	TRAV35	5/5
	CAGLNSGGSNYKLTF	TRAV35	3/5
	CAASGARGAQKLVF	TRAV29/DV5	2/5
$S_{751-765}$	CAASIAGSARQLTF	TRAV13-1	3/6
	CVVNARSSNTGKLIF	TRAV12-1	5/6
	CVVNIGSSASKIIF	TRAV12-1	5/6
	CVVNKRSSSASKIIF	TRAV12-1	3/6
	CVVNRGGYQKVTF	TRAV12-1	3/6
	CAASISGGYNKLIF	TRAV13-1	2/6
	CATGGSNYKLTF	TRAV17	3/6
	CAVGRYGGSQGNLIF	TRAV2	3/6
	CVVNKYSSNTGKLIF	TRAV12-1	2/6
	CVVNPKTSYDKVIF	TRAV12-1	2/6
	CVVNRGYSTLTF	TRAV12-1	2/6
	CVVPTGGGNKLTF	TRAV12-1	2/6
$S_{866-880}$	CAGTGNNRKLIW	TRAV25	6/6
	CAVAGNNRKLIW	TRAV25	3/6
	CIVRAANQAGTALIF	TRAV26-1	3/6
	CIVRVEYNFNKFYF	TRAV26-1	4/6
	CVASGGSNYKLTF	TRAV12-1	3/6
	CAFMKPVTQGAQKLVF	TRAV38-1	2/6
	CILRAPLSFGNEKLTF	TRAV26-2	2/6
	CIVRGLNAGNMLTF	TRAV26-1	2/6
	CIVRVGGSWGKLQF	TRAV26-1	2/6
	CIVRVLFGNEKLTF	TRAV26-1	2/6
	CIVRVLGGGYNKLIF	TRAV26-1	2/6
	CVVNPNARLMF	TRAV12-1	4/6
	CVVNRGSNYQLIW	TRAV12-1	2/6
	CVVNRGSSYKLIF	TRAV12-1	3/6
	CVVSGGSNYKLTF	TRAV12-1	3/6

Epitope	CDR3β	TRBV	No. of patients
$S_{166-180}$	CASSFRGDGYTF	TRBV5-1	2/5
	CASSPRDRVNTGELFF	TRBV9	2/5
	CASSQGVGYTF	TRBV4-1	2/5
	CASSYRGAYGYTF	TRBV6-2	2/5
	CASSYSGGQPQHF	TRBV6-5	2/5
	CAWRGGIGYTF	TRBV30	2/5
$S_{751-765}$	CASSEGAGSQPQHF	TRBV6-1	4/5
	CASSSSGGGSYEQYF	TRBV6-5	2/5
	CASSTPNRGNNQPQHF	TRBV19	2/5
	CASTEGASNQPQHF	TRBV6-1	2/5
$S_{866-880}$	CASSPLANEQFF	TRBV11-2	3/6
	CASSPTYEQYF	TRBV11-2	3/6
	CASSFGGSYGYTF	TRBV12-3	3/6
	CASSFGGNYGYTF	TRBV12-4	2/6
	CASSQVAAEQFF	TRBV3-1	3/6
	CASSLGPNSGNTIYF	TRBV5-1	2/6
	CASSLLTGSTDTQYF	TRBV5-1	2/6
	CASSLSGLDGYTF	TRBV5-1	2/6
	CASSLVSEKLFF	TRBV11-2	2/6
	CASSQVGAGTDTQYF	TRBV4-3	2/6

Epitope	CDR3_alpha	TRAV	CDR3_beta	TRBV	No of patients
$S_{166-180}$	CAGMNYGGSQGNLIF	TRAV35	CASSQGVGYTF	TRBV4-1	2/5
	CAGMNYGGSQGNLIF	TRAV35	CASSYRGAYGYTF	TRBV6-2	2/5
	CAGMNYGGSQGNLIF	TRAV35	CAWRGGIGYTF	TRBV30	2/5
	CAGQLYGGSQGNLIF	TRAV35	CASSFRGDGYTF	TRBV5-1	2/5
	CAGQLYGGSQGNLIF	TRAV35	CASSYSGGQPQHF	TRBV6-5	2/5
$S_{751-765}$	CVVNKGSSASKIIF	TRAV12-1	CASSEGASNQPQHF	TRBV6-1	4/6
$S_{866-880}$	CAGTGNNRKLIW	TRAV25	CASSFGAYGYTF	TRBV12-4	2/6
	CAGTGNNRKLIW	TRAV25	CASSFGGNYGYTF	TRBV12-3	2/6
	CAMNGGANSKLTF	TRAV12-3	CASSLGPNSGNTIYF	TRBV5-1	2/6
	CAVAGNNRKLIW	TRAV25	CASSQVGAGTDTQYF	TRBV4-3	2/6
	CIVRAANQAGTALIF	TRAV26-1	CASSQVAGEQYF	TRBV3-1	3/6
	CIVRVEYNFNKFYF	TRAV26-1	CASSPLANEQFF	TRBV11-2	3/6
	CIVRVSYNFNKFYF	TRAV26-1	CASSLVSEKLFF	TRBV11-2	2/6
	CVVNRGSSYKLIF	TRAV12-1	CASSQTYEQYF	TRBV11-2	3/6

Figures

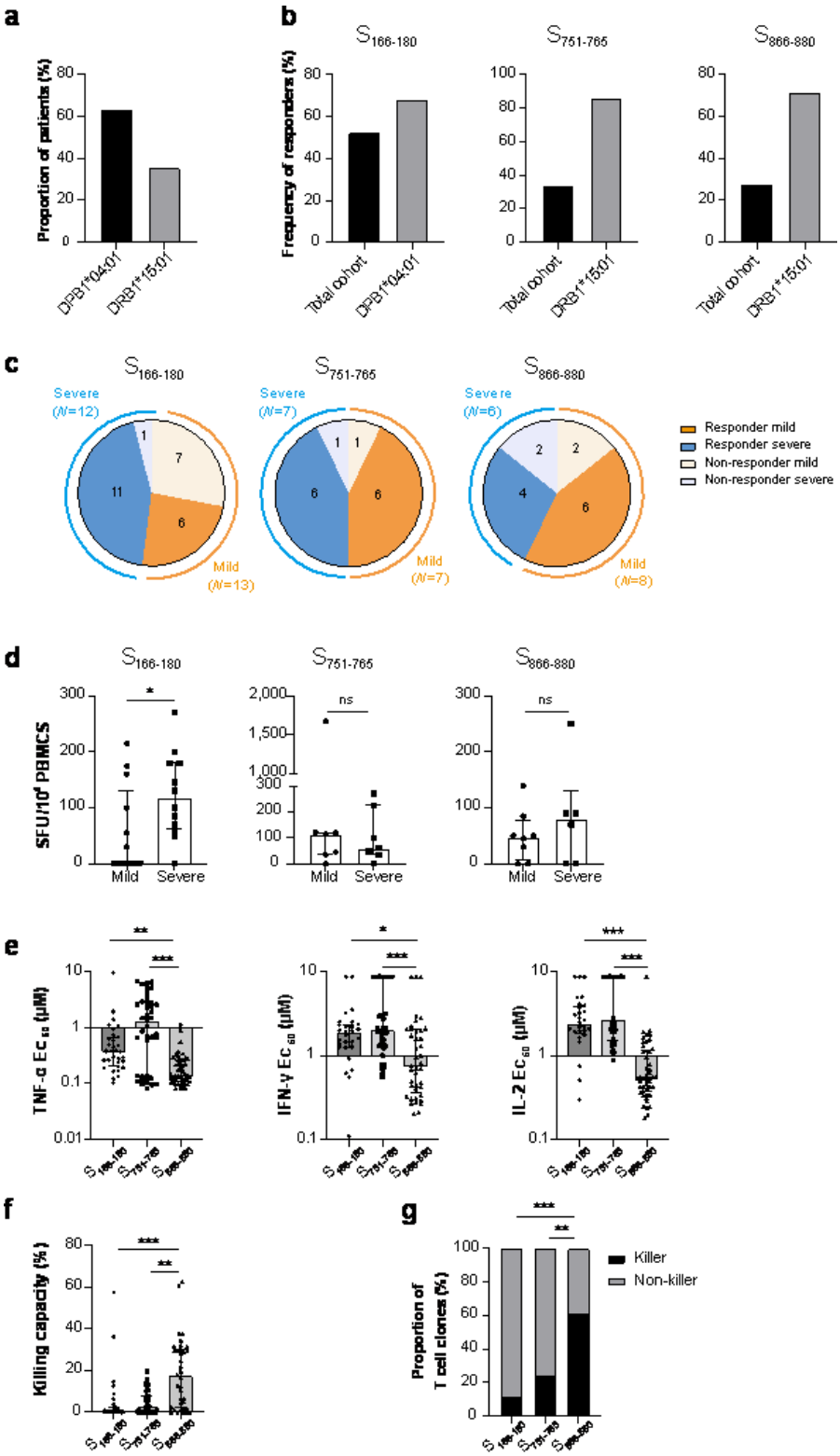

Figure 1

Frequency and magnitude of response to $S_{166-180}$-DPB1*04:01, $S_{751-765}$-DRB1*15:01 and $S_{866-880}$-DRB1*15:01 epitopes in COVID-19 patients. (a) Proportion of patients with HLA-DPB1*04:01 and DRB1*15:01 in overall cohort (*n* = 45). **(b)** Frequency of convalescent COVID-19 patients with T cells responding to $S_{166-180}$ (*n* =21/40), $S_{751-765}$-DRB1*15:01 (*n* = 12/37) or $S_{866-880}$-DRB1*15:01 (*n* = 10/36) peptide stimulation. **(c)** Proportion of DPB1*04:01 and DRB1*15:01 positive patients responding to S_{166-}

$_{180}$, $S_{751-765}$ and $S_{866-880}$ (n = 17, 12, 10 respectively), and non-responders (n = 8, 2, 4 respectively) with mild or severe COVID-19 disease. **(d)** Comparison of the magnitude of responses to $S_{166-180}$, $S_{751-765}$ and $S_{866-880}$ epitopes between mild and severe DPB1*04:01 (n = 13, n = 12, P = 0.031) or DRB1*15:01 positive responders ($S_{751-765}$: n = 7, n = 7, P = 0.878; $S_{866-880}$: n = 8, n = 6, P = 0.470). **(e)** Comparison of cytokine production (TNF-α, IFN-γ and IL-2) upon stimulation with each of the three spike peptides. P values were as follows: TNF-α: P = 0.820 for $S_{166-180}$ vs $S_{751-765}$; P = 0.001 for $S_{166-180}$ vs $S_{866-880}$; P < 0.001 for $S_{751-765}$ vs $S_{866-880}$; IFN-γ: P = 0.334 for $S_{166-180}$ vs $S_{751-765}$; P = 0.038 for $S_{166-180}$ vs $S_{866-880}$; P < 0.001 for $S_{751-765}$ vs $S_{866-880}$; IL-2: P = 1.000 for $S_{166-180}$ vs $S_{751-765}$; P < 0.001 for $S_{166-180}$ vs $S_{866-880}$; P < 0.001 for $S_{751-765}$ vs $S_{866-880}$. **(f)** Comparison of killing capacity (%) across each spike-specific $CD4^+$ T cell. P = 0.251 for $S_{166-180}$ vs $S_{751-765}$; P < 0.001 for $S_{166-180}$ vs $S_{866-880}$; P = 0.001 for $S_{751-765}$ vs $S_{866-880}$. **(g)** Proportion of $CD4^+$ T cell clones that can be divided as “killer” (black) or “non-killer” (grey) $CD4^+$ T cells. P = 0.170 for $S_{166-180}$ vs $S_{751-765}$; P < 0.001 for $S_{166-180}$ vs $S_{866-880}$; P = 0.001 for $S_{751-765}$ vs $S_{866-880}$. Data are presented as medians with interquartile ranges (IQRs) (**d**, **e** and **f**). The Mann-Whitney U-test was used to compare distributions of two groups and Kruskal-Wallis one-way ANOVA for comparison among three groups, while ratio was compared using Chi-square test, and the two-tailed P value was calculated. ns not significant, *P<0.05, **P<0.01, *** P<0.001. SFU, spot-forming units.

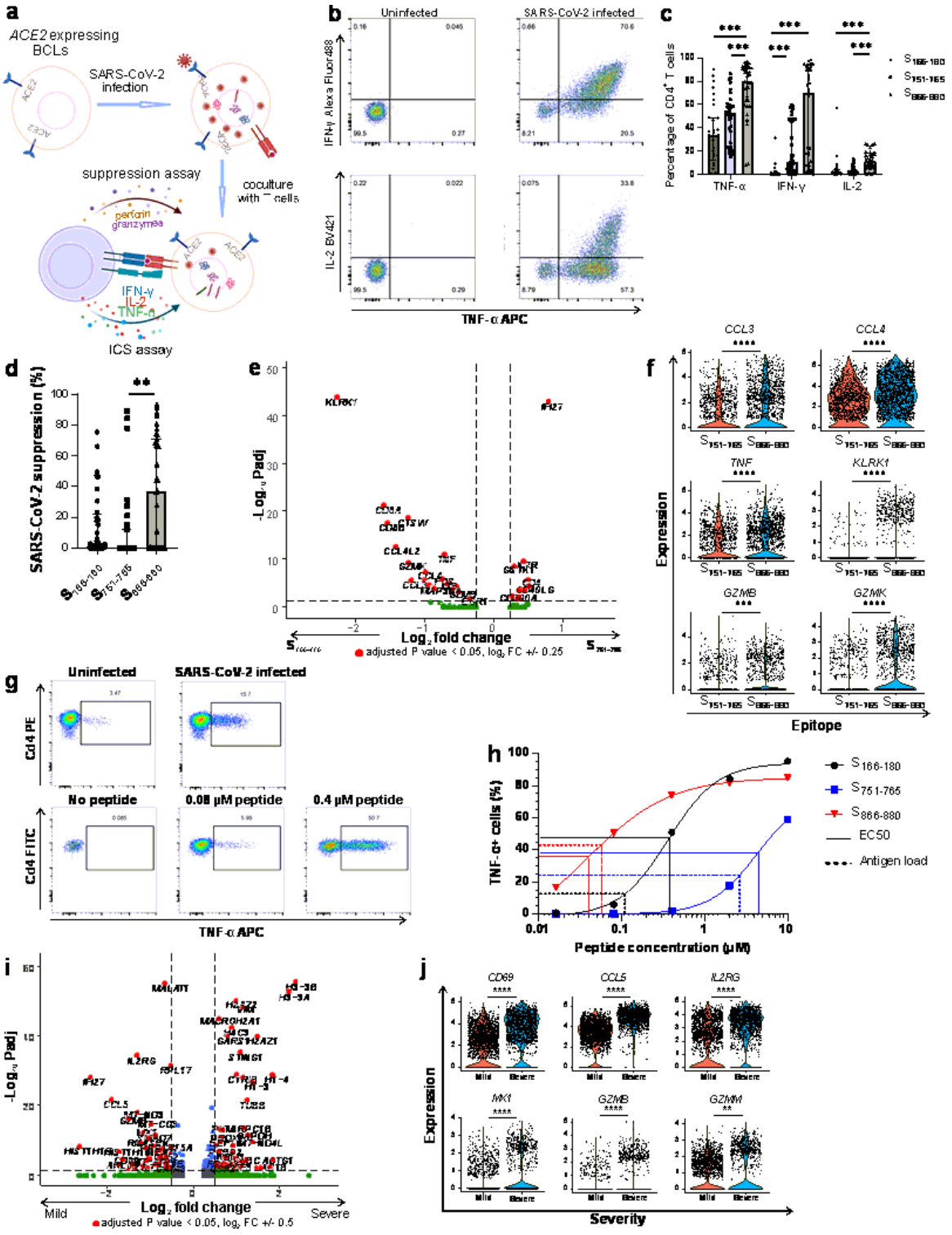

Figure 2

Variation between spike epitope specific CD4⁺ T cells and antiviral effector function. (a) Schematic diagram detailing workflow of viral suppression and intracellular cytokine assays. **(b)** Representative ICS flow cytometry plots measuring TNF-α, IFN-γ and IL-2 expression in CD4⁺ T cells incubated with SARS-CoV-2 infected antigen presenting BCLs. **(c)** ICS data summarised for each epitope as percentage of CD4⁺ T cells expressing each cytokine. TNF-α: $P = 0.178$ for $S_{166\text{-}180}$ vs $S_{751\text{-}765}$; $P < 0.001$ for $S_{166\text{-}180}$ vs

$S_{866-880}$; $P < 0.001$ for $S_{751-765}$ vs $S_{866-880}$; IFN-γ: $P < 0.001$ for $S_{166-180}$ vs $S_{751-765}$; $P < 0.001$ for $S_{166-180}$ vs $S_{866-880}$; $P = 0.071$ for $S_{751-765}$ vs $S_{866-880}$; IL-2: $P = 1.000$ for $S_{166-180}$ vs $S_{751-765}$; $P < 0.001$ for $S_{166-180}$ vs $S_{866-880}$; $P < 0.001$ for $S_{751-765}$ vs $S_{866-880}$. **(d)** Comparison of SARS-CoV-2 viral suppression across spike-specific $CD4^+$ T cells. $P = 0.305$ for $S_{166-180}$ vs $S_{751-765}$; $P = 0.241$ for $S_{166-180}$ vs $S_{866-880}$; $P = 0.002$ for $S_{751-765}$ vs $S_{866-880}$. **(e)** Differentially expressed genes between $S_{751-765}$- (*n* = 1629*)* and $S_{866-880}$-specific (*n* = 2233) single cells from 5 patients. **(f)** Violin plots showing gene expression for *CCL3* ($P = 2.79 \times 10^{-6}$), *CCL4* ($P = 4.4 \times 10^{-8}$), *TNF* ($P = 9.08 \times 10^{-12}$), *KLRK1* ($P = 1.37 \times 10^{-44}$), *GZMK* ($P = 5.13 \times 10^{-10}$) and *GZMB* ($P = 6.13 \times 10^{-4}$). **(g)** Representative flow cytometry plots measuring TNF-α expression after incubation with SARS-CoV-2 infected cells or peptide-loaded target cells. **(h)** Estimated antigen load of each epitope on virus infected cells and EC_{50} of T cell response. $S_{166-180}$ is shown as black circles, $S_{751-765}$ in blue squares and $S_{866-880}$ in red triangles. Dashed lines represent the estimated antigen-load of each corresponding epitope on virus-infected cells whereas solid lines show the EC_{50} of each T cell response. **(i)** Differentially expressed genes between single cells from mild (*n* = 2 patients and 2728 cells) and severe (*n* = 2 patients and 1823 cells) convalescent COVID-19 patients ($S_{751-765}$- and $S_{866-880}$-specific $CD4^+$ T cells). **(j)** Violin plots showing gene expression for *CD69* ($P = 2.75 \times 10^{-5}$), *CCL5* ($P = 1.61 \times 10^{-22}$), *IL2RG* ($P = 3.27 \times 10^{-35}$), *MX1* ($P = 3.76 \times 10^{-13}$), *GZMB* ($P = 6 \times 10^{-17}$) and *GZMM* ($P = 3.87 \times 10^{-3}$. Data are presented as medians with interquartile ranges (IQRs) (**c** and **d**). Kruskal-Wallis one-way ANOVA was used for analysis and the two-tailed *P* value was calculated. MAST statistical test was used with sequencing batches as latent variable (**e** and **i**). Adjusted *P* values are shown (**f** and **j**). ns, not significant, *$P < 0.05$, **$P < 0.01$, *** $P < 0.001$, **** $P < 0.0001$. ICS, intracellular cytokine staining; BCLs, B cell lines.

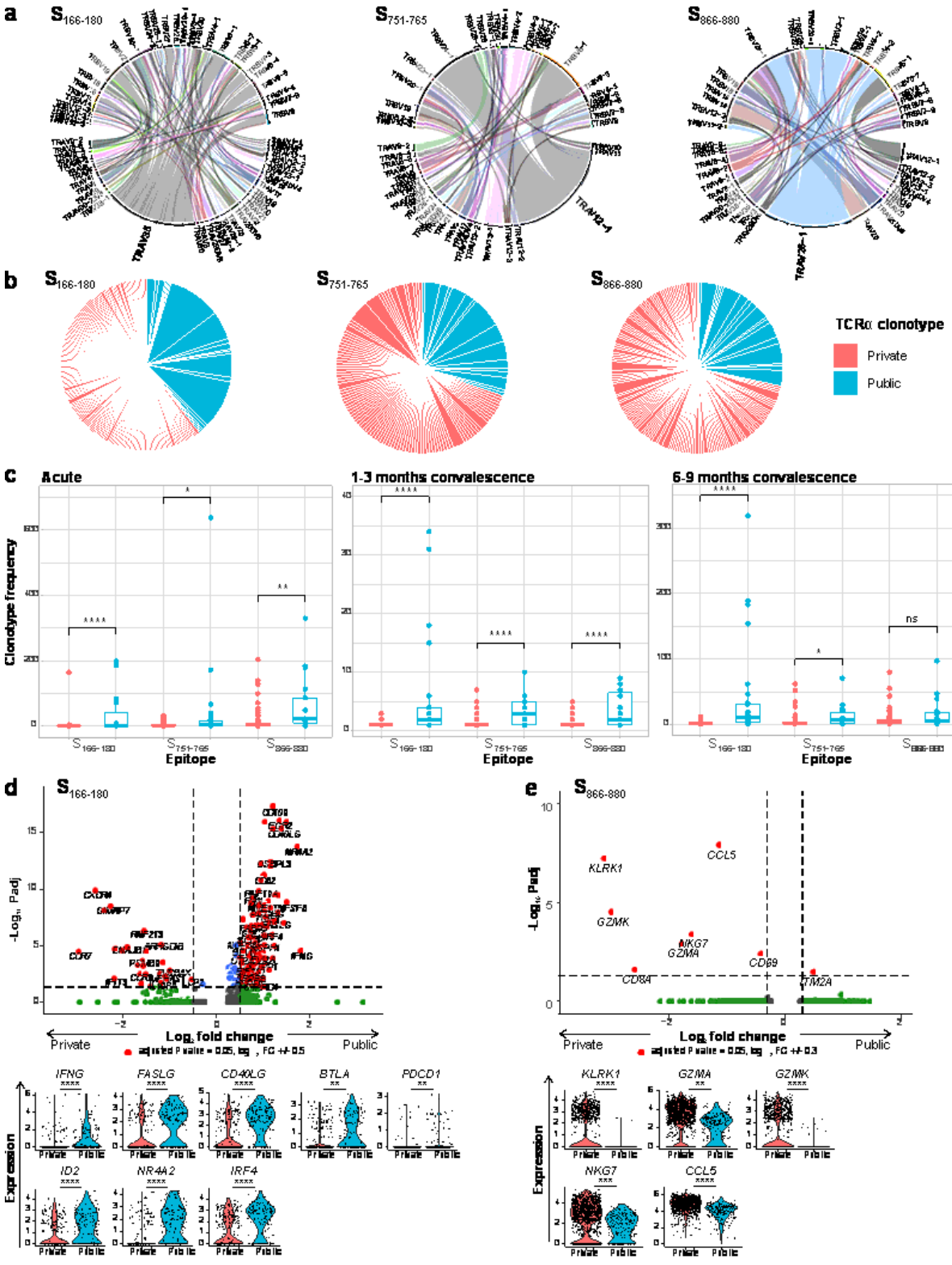

Figure 3

TCR repertoire of $S_{166-180}$-DPB1*04:01, $S_{751-765}$-DRB1*15:01 and $S_{866-880}$-DRB1*15:01 specific CD4$^+$ T cells from COVID-19 patients. (a) Circos plots for each epitope depicting V αβ gene usage at 1 month convalescence (*n* = 5 patients and 152 $S_{166-180}$ cells, *n* = 4 patients and 77 $S_{751-765}$ cells, *n* = 4 patients and 100 $S_{866-880}$ cells). **(b)** Pie charts depicting Vα clonotypes from 1 month convalescence for each

epitope (*n* = 216 $S_{166-180}$ clonotypes, *n* = 117 $S_{751-765}$ clonotypes, *n* = 151 $S_{866-880}$ clonotypes) with public (blue) and private (red) clonotypes highlighted. **(c)** Comparison between frequencies of public and private clonotypes for each epitope from T cells sampled from patients at different timepoints (*n* = 3 patients and 335 acute clonotypes, *n* = 4-5 patients and 484 1-3 months clonotypes and *n* = 3 patients and 286 6/9 months clonotypes from convalescent disease). Public v private acute: $S_{166-180}$ $P = 1.7 \times 10^{-6}$, $S_{751-765}$ $P = 0.04$, $S_{866-880}$ $P = 0.0098$; 1-3 months: $S_{166-180}$ $P = 1.4 \times 10^{-15}$, $S_{751-765}$ $P = 6.3 \times 10^{-8}$, $S_{866-880}$ $P = 3.8 \times 10^{-6}$; 6-9 months: $S_{166-180}$ $P = 3.1 \times 10^{-9}$, $S_{751-765}$ $P = 0.026$, $S_{866-880}$ $P = 0.15$. Adjusted *P* values are shown (Benjamini-Hochberg). **(d)** Differentially expressed genes from $S_{166-180}$ single cells from 1 month convalescence (*n* = 5 patients) between T cells with public (*n* = 128) or private (*n* = 285) clonotypes. Violin plots showing gene expression for *IFNG* ($P = 2.92 \times 10^{-5}$), *FASLG* ($P = 9 \times 10^{-8}$), *CD40LG* ($P = 4.86 \times 10^{-16}$), *BTLA* ($P = 1.48 \times 10^{-3}$), *PDCD1* ($P = 1.61 \times 10^{-3}$), *ID2* ($P = 1.07 \times 10^{-5}$), *NR4A2* ($P = 1.94 \times 10^{-14}$) and *IRF4* ($P = 1.18 \times 10^{-6}$). (**e**) Differentially expressed genes from $S_{866-880}$ single cells from 6 and 9 months convalescence (*n* = 5 patients) between T cells with public (*n* = 194) or private (*n* = 1325) clonotypes. Violin plots showing gene expression for *KLRK1* ($P = 5.65 \times 10^{-8}$), *GZMA* ($P = 1.22 \times 10^{-3}$), *GZMK* ($P = 2.95 \times 10^{-5}$), *NKG7* ($P = 3.92 \times 10^{-4}$) and *CCL5* ($P = 1.19 \times 10^{-8}$). For boxplots, the lower and upper hinges represent the 25-75th percentiles, the central line represents the median, and the whiskers extend to the maximum and minimum values that are no greater than 1.5x the IQR. The MAST statistical test was used with sequencing batch as latent variable. Adjusted *P* values are shown. ns, not significant; * $P < 0.05$, ** $P < 0.01$, **** $P < 0.001$, **** $P < 0.0001$.

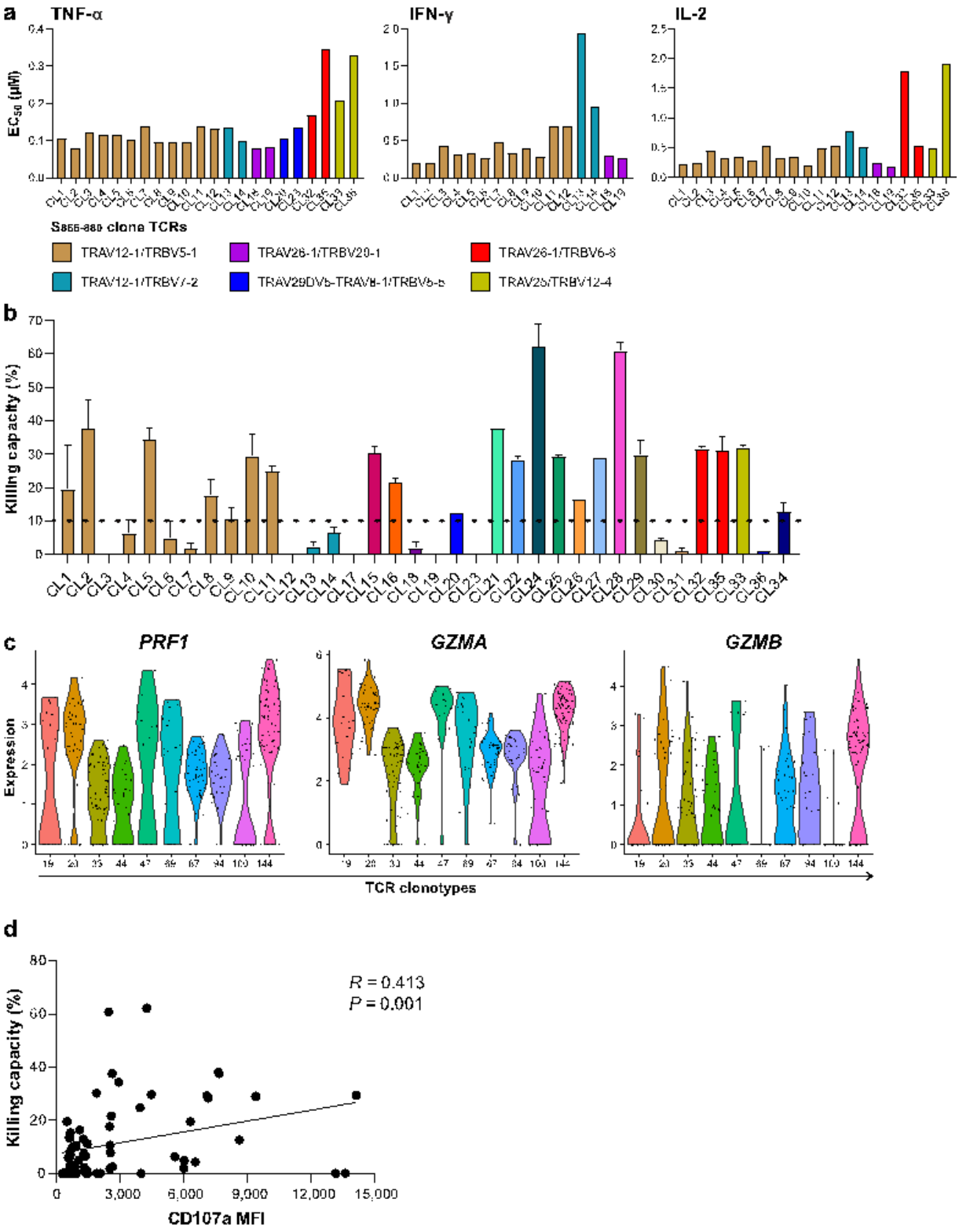

Figure 4

Functionality and antiviral efficacy of $S_{866-880}$-specific $CD4^+$ T cells rely on factors other than TCR usage. (a) EC_{50} concentrations for IFN-γ, IL-2 and TNF-α production by T cell clones with identical TCRs. **(b)** Killing capacity of T cell clones with the same TCRs. Bar colours match figure legend from (a), other colours not shown in legend depict other TCRs. **(c)** Expression of cytotoxic molecules *PRF1*, *GZMA*

and *GZMB* on single cells with same TCRs (tetramer-sorted $S_{866-880}$ single cells from 4 patients, $n = 399$ cells total). **(d)** Association between T cell killing and CD107a expression. ($n = 72$, $R = 0.413$, $P = 0.001$); Data are presented as medians with interquartile ranges (IQRs). Correlation analysis was performed using Spearman's rank correlation coefficient. The Mann-Whitney *U*-test was used for analysis and the two-tailed P value was calculated. n.s. not significant, *$P<0.05$, **$P<0.01$, *** $P<0.001$. MFI, median fluorescent intensity.

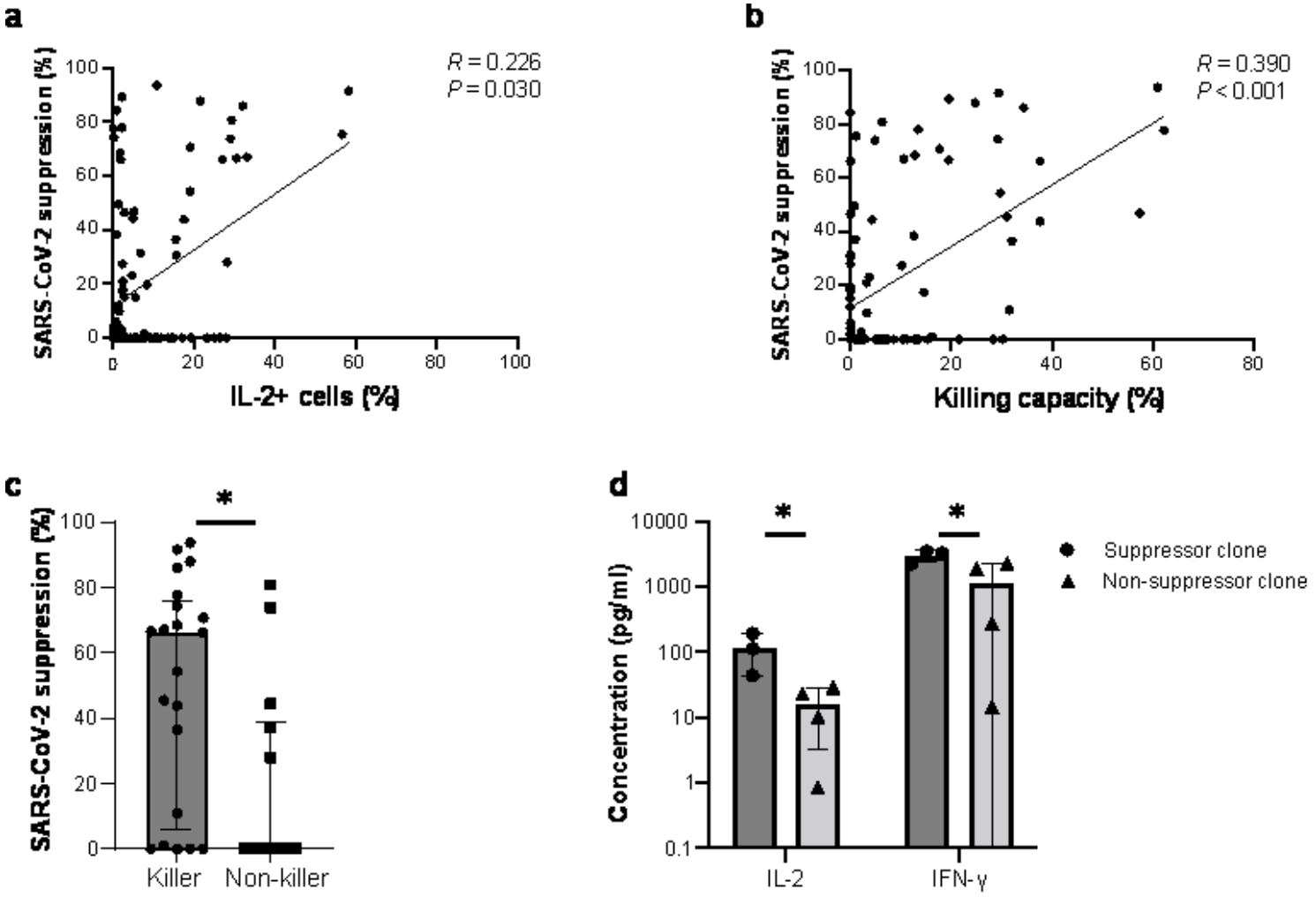

Figure 5

Viral suppression by spike-specific CD4$^+$ T cells is correlated with killing and IL-2 production.
(a) Correlation of virus suppression with proportion of cells producing IL-2 ($n = 93$, $R = 0.226$, $P = 0.030$). **(b)** Correlation of virus suppression with cell killing capacity of T cells ($n = 98$, $R = 0.390$, $P < 0.001$). **(c)** Comparison of virus suppression between $S_{866-880}$-specific CD4$^+$ killer cells ($n = 21$) and non-killer cells ($n = 14$), $P = 0.010$. **(d)** Comparison of cytokine production of CD4+ non-killer cells with virus suppression (suppressor clone, $n = 3$) and without virus suppression (non-suppressor clone, $n = 4$). $P = 0.040$ for IFN-γ, $P = 0.040$ for IL-2. Data are presented as medians with interquartile ranges (IQRs) in **c** and means ± standard deviations (SD) in **d**. Correlation analysis was performed using Spearman's rank

correlation coefficient. The Mann-Whitney *U*-test and independent-samples t-test was used for analysis and the two-tailed P value was calculated. *$P < 0.05$.

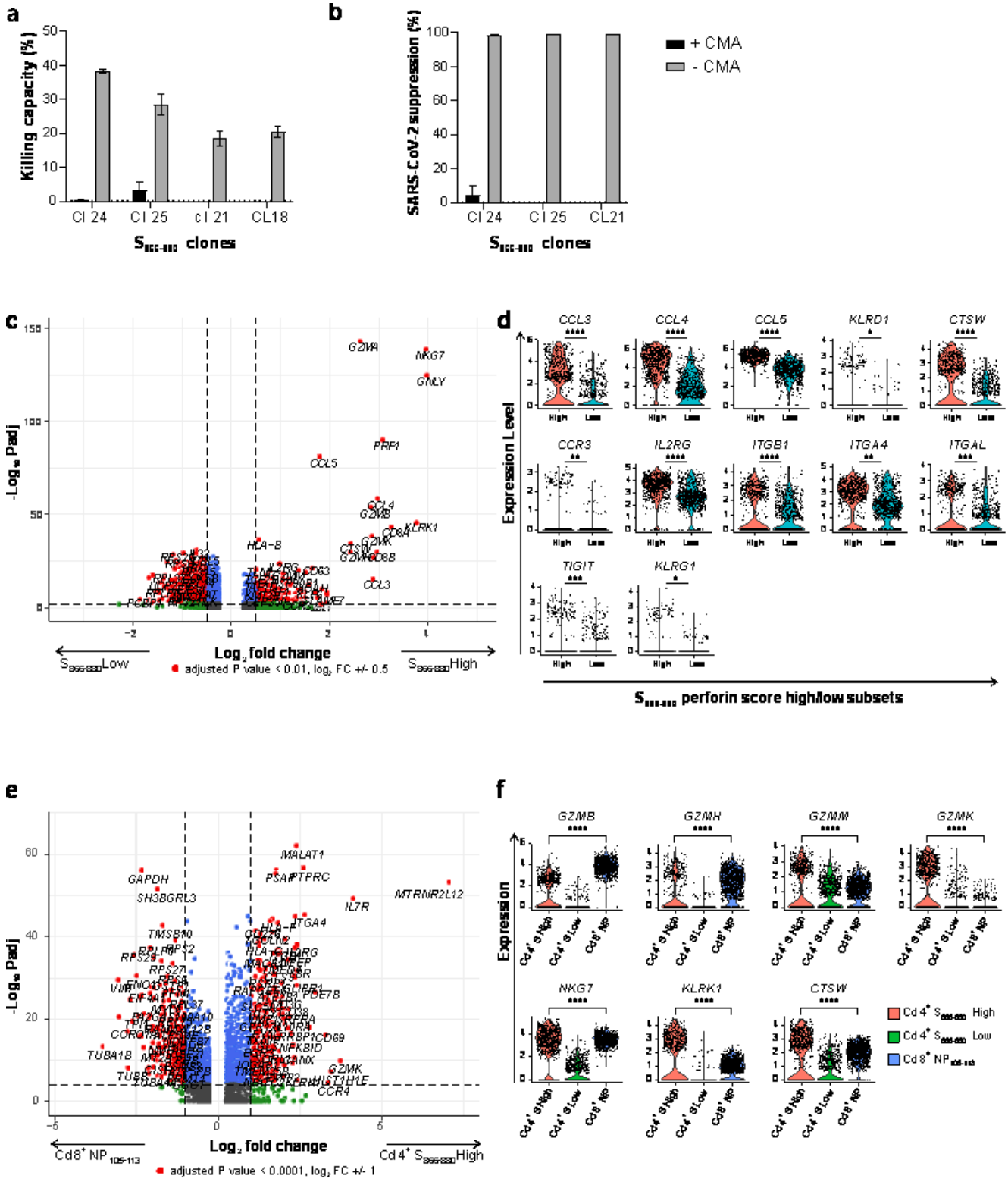

Figure 6

Cytotoxicity of spike-specific CD4$^+$T cells is partially mediated through perforin. (a) T cell killing and (**b**) virus suppression by $S_{866-880}$ T cell clones with and without CMA treatment. **(c)** Comparison of gene

expression between $S_{866-880}$-specific $CD4^+$ single T cells (*n* = 5 patients) with high perforin score (*n* = 693) and low perforin score (*n* = 724). **(d)** Differentially expressed genes between T cells with high and low perforin score. Violin plots showing gene expression for *CCL3* (*P* = 8.48 x 10^{-16}), *CCL4* (*P* = 2.26 x 10^{-59}), *CCL5* (*P* = 9.29 x 10^{-82}), *KLRD1* (*P* = 2.01 x10^{-2}), *CTSW* (*P* = 6.54 x 10^{-35}), *CCR3* (P = 4.6 x 10^{-3}), *IL2RG* (*P* = 3.17 x 10^{-24}), *ITGB1* (*P* = 1.19 x 10^{-8}), *ITGA4* (*P* = 1.26 x 10^{-3}), *ITGAL* (*P* = 3.78 x 10^{-4}), *TIGIT* (*P* = 2.82 x 10^{-4}), *KLRG1* (*P* = 1.94 x 10^{-2}). **(e)** Comparison of gene expression between $S_{866-880}$-specific $CD4^+$ T cells with high perforin score (*n* = 5 patients and 693 cells) and tetramer-sorted HLA-B*07:02/NP_{105}-specific $CD8^+$ CTLs (*n* = 3 patients and 1041 cells). (**f**) Differentially expressed genes between $CD4^+$ T cells with high perforin score (*n* = 5 patients, 693 cells), $CD4^+$ T cells with low perforin score (*n* = 5 patients, 724 cells) and $CD8^+$ CTLs (*n* = 3 patients, 1041 cells). Violin plots showing gene expression for *GZMB* (*P* = 2.24 x 10^{-25}), *GZMH* (*P* = 2.09 x 10^{-5}), *GZMK* (*P* = 1.78 x 10^{-10}), *GZMM* (*P* = 1.91 x 10^{-10}), *NKG7* (P = 9.51 x 10^{-12}), *KLRK1* (*P* = 8.3 x 10^{-6}), and *CTSW* (*P* = 2.86 x 10^{-11}). The MAST statistical test was used for analysis with sequencing batch as latent variable and the two-tailed *P* value was calculated, adjusted *P* values are shown. * *P* < 0.05, ** *P* < 0.01, *** *P* < 0.001, **** *P* < 0.0001.

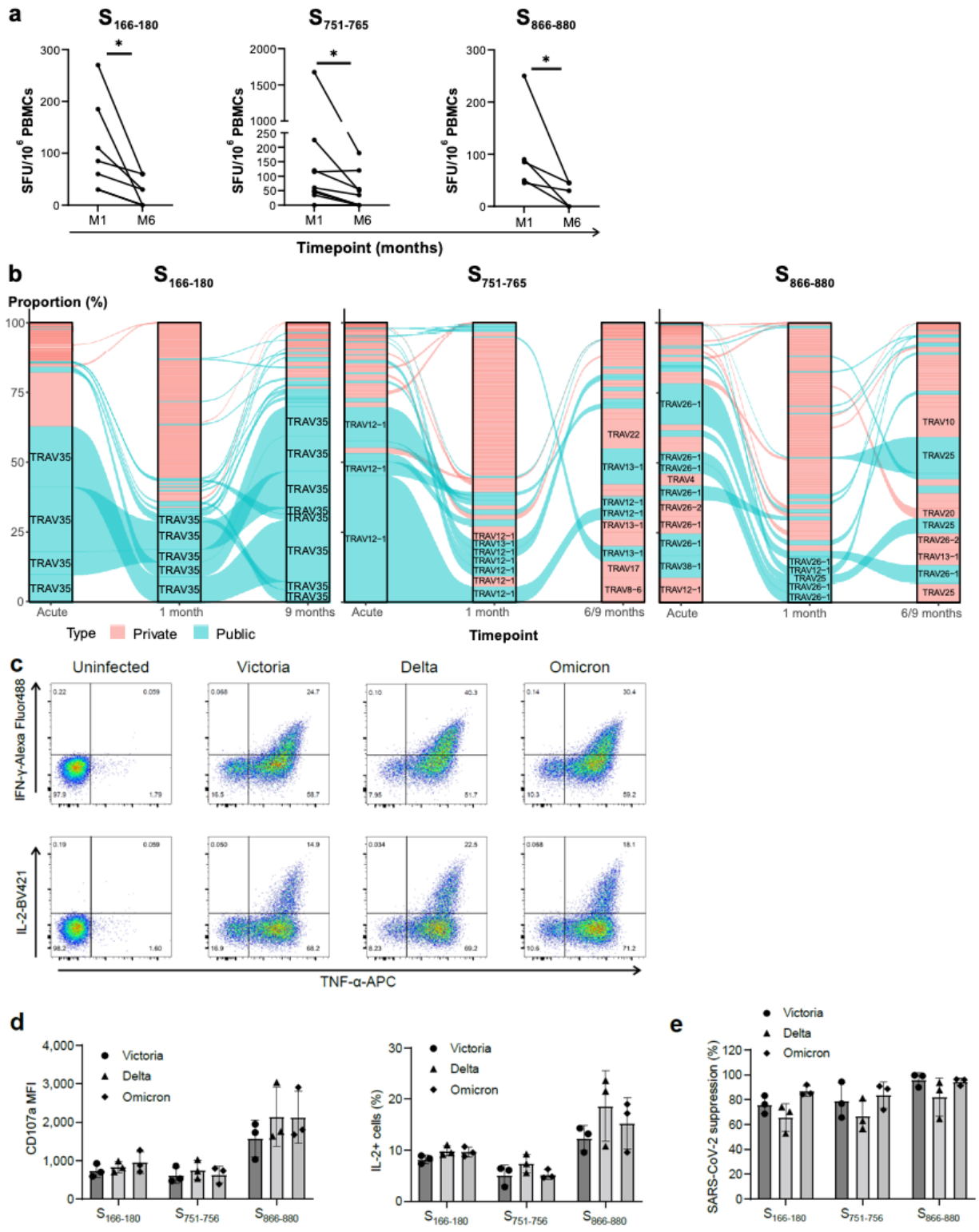

Figure 7

Characterization of $S_{166-180}$-DPB1*04:01, $S_{751-765}$-DRB1*15:01 and $S_{866-880}$-DRB1*15:01 specific CD4$^+$ T cell response at six to nine months convalescence. (**a**) Comparison of $S_{166-180}$, $S_{751-765}$ and $S_{866-880}$-specific CD4$^+$ T cell response between 1 and 6 months of convalescence. $S_{166-180}$: $n = 7$, $P = 0.017$; $S_{751-765}$: $n = 9$, $P = 0.017$; $S_{866-880}$: $n = 5$, $P = 0.043$. (**b**) TCR repertoires of $S_{166-180}$, $S_{751-765}$ and $S_{866-880}$-

specific $CD4^+$ T cell response at acute infection, 1 month and 6/9 months convalescence. TCR clonotypes coloured pink and blue are private TCRs and public TCRs, respectively. For clarity only TRAV gene usage is shown rather than full α clonotype (CDR3α amino acid sequence + TRAV). (**c**) Representative ICS flow cytometry plots measuring TNF-α, IFN-γ, and IL-2 expression on bulk $S_{866-880}$-specific T cell lines from C-COV19-064 at 6 months incubated with BCLs infected with SARS-CoV-2 Victoria, Delta or Omicron variants (uninfected BCLs shown as negative control). (**d**) CD107a MFI and IL-2+ cell population in $S_{166-180}$, $S_{751-765}$ and $S_{866-880}$- specific $CD4^+$ T cell bulk lines at 6 - 9 months when cocultured with BCLs infected with SARS-CoV-2 Victoria, Delta or Omicron variants. Data represent one of two independent experiments with similar results. **(e)** Inhibition of SARS-CoV-2 replication by $S_{166-180}$, $S_{751-765}$ and $S_{866-880}$- specific $CD4^+$ T cell bulk lines at 6-9 months. Single representative experiment shown as means ± S.D. MFI, median fluorescent intensity. Wilcoxon matched-pair signed-rank was used to compare T cell responses between month1 and month6. *$P < 0.05$.

Supplementary Files

This is a list of supplementary files associated with this preprint. Click to download.

- SupplementaryInformation.docx
- SupplementaryTable1.xlsx
- SupplementaryTable2.xlsx